Journal of Biomedical Optics 9(6), 1327–1335 (November/December 2004)

Photoacoustic imaging of blood vessels with a double-ring sensor featuring a narrow angular aperture

Roy G. M. Kolkman
Erwin Hondebrink
Wiendelt Steenbergen
Ton G. van Leeuwen
Frits F. M. de Mul
University of Twente
Biophysical Engineering
Faculty of Science and Technology
P.O. Box 217
7500 AE Enschede
The Netherlands
E-mail: r.g.m.kolkman@utwente.nl

Abstract. A photoacoustic double-ring sensor, featuring a narrow angular aperture, is developed for laser-induced photoacoustic imaging of blood vessels. An integrated optical fiber enables reflection-mode detection of ultrasonic waves. By using the cross-correlation between the signals detected by the two rings, the angular aperture of the sensor is reduced by a factor of 1.9, from 1.5 to 0.8 deg. Consequently, photoacoustic images could be obtained in a manner analogous to the ultrasound B-scan mode. Next, the cross section of artificial blood vessels is visualized by reconstruction of the absorbed energy distribution. Finally, *in vivo* imaging and the subsequent reconstruction of the absorbed energy distribution is demonstrated for superficial blood vessels in the human wrist. [DOI: 10.1117/1.1805556]

Keywords: optoacoustic; imaging; cross-correlation; blood vessel; *in vivo*.

Paper 03145 received Dec. 3, 2003; revised manuscript received Mar. 5, 2004; accepted for publication Mar. 22, 2004.

1 Introduction

Biomedical photoacoustic imaging is a hybrid imaging technique that uses pulsed light to generate acoustic waves in tissue. When this pulsed light is absorbed in the tissue, a small temperature rise will occur that causes thermal expansion. As a result, a thermoelastic pressure transient is generated, whose amplitude is dependent on the amount of absorbed light, determined by the local energy fluence [J/m^2] and the optical absorption coefficient of the target. The advantage of photoacoustic imaging over purely optical techniques is that the preceding path of the light is not relevant. Furthermore, the resolution is dependent on the geometry of the ultrasound-detection system together with the image reconstruction algorithm, and is not limited by the large amount of scattering of light in tissue.

Hoelen et al.[1] showed that photoacoustics can be used to perform high-resolution 3-D imaging of artificial blood vessels in a tissue phantom with ~20-μm depth resolution and ~200-μm resolution in a lateral direction. Pilatou et al.[2] applied this method to image a vascular tree from a Wistar rat *in vitro*. Photoacoustics is also used to perform *in vivo* tomographic imaging on small animals. Kruger et al. reported 2-D photoacoustic images[3] as well as slices of a 3-D photoacoustic image[4] of sacrificed mice. Wang et al.[5,6] developed a system capable of performing photoacoustic structural and functional imaging in a rat brain. Other applications of photoacoustics include, e.g., the development of a laser optoacoustic imaging system (LOIS) for breast cancer detection (Oraevsky et al.[7]), the development of a photoacoustic probe for port-wine stain depth measurements (Viator et al.[8]), the characterization of layered tissue structures in the near- and far-field (Paltauf and Schmidt-Kloiber[9]), or determination of optical properties of soft tissue in the near infrared using photoacoustic spectroscopy (Köstli et al.[10]).

Acoustic waves in tissue can be detected by measurement of the pressure transient or displacement at the tissue surface. Measurement of these pressure transients using piezoelectric sensors is the most commonly used method in photoacoustics.[11–15] Although optical methods for detection of acoustic waves have been developed as well,[16–20] piezoelectric sensors have the advantage that broadband piezoelectric sensors are easier to construct and have a slightly better sensitivity than optical detection systems.[15] The shape and size of the piezoelectric element determine the characteristics, such as the angular aperture and the frequency response of the sensor. Here, ''angular aperture'' denotes the arctan of half-width at half maximum (HWHM) of the directional sensitivity curve over the depth of the detector. Sensors with a small element size (point sensors) have a very large angular aperture and thus are able to detect acoustic signals originating from a large volume in the tissue.[1,12] Consequently, time domain[21,22] or frequency domain[23,24] reconstruction algorithms are needed to reconstruct the image. In contrast, for sensors with a narrow angular aperture, e.g., ring-shaped or annular sensors,[25,26] the time traces can be regarded as 1-D depth images [amplitude (A) scans] of photoacoustic sources inside the measurement volume. Comparable to an echographic B scan, imaging with such a ring-shaped sensor is carried out by scanning the sensor over the tissue surface, permitting real-time reconstruction of the corresponding part of the image without the need of information of adjacent sensor positions.

Recently, we have imaged the joining of two human palmar veins *in vivo* using a double-ring sensor.[11] In this work the characteristics of this double-ring sensor together with a cross-correlation method that reduces its angular aperture are

Address all correspondence to Roy G. M. Kolkman, University ot Twente, Biophysical Engineering, Faculty of Science and Technology, P.O. Box 217, NL-7500 AE Enschede, Netherlands. Tel: 31-53-489-3870; Fax: 31-53-489-1105; E-mail: r.g.m.kolkman@utwente.nl

1083-3668/2004/$15.00 © 2004 SPIE

presented. Imaging in 2-D with this sensor is demonstrated in phantoms as well as *in vivo*.

2 Theory

In this section, the theoretically expected directional sensitivity of a double-ring photoacoustic sensor, consisting of two concentric ring-shaped sensor areas, is calculated. The inner ring of this sensor has an inner radius of 2 mm and a width of 0.17 mm. The outer ring has an inner radius of 3.5 mm and a width of 0.1 mm, so the detection area of both rings is equal.

The response of the sensor was characterized by calculating the voltage response of a piezoelectric (photo-) acoustic sensor to a pressure transient $P(r,t)$ [Eq. (1)]. This equation holds for piezoelectric sensors for which only the thickness mode is relevant (only taking into account pressure contributions into the poling direction) and when the thickness d of the piezo is small compared to the acoustic wavelength λ_a (i.e., $d<1/4\lambda_a$).

$$V_{\text{piezo}}(t)=\frac{g_{33}d}{A}\int_A P(r,t)T_A(r)\cos[\theta_t(r)]dA, \qquad (1)$$

where g_{33}[V/(Pa·m)] is the piezoelectric voltage constant (describing the magnitude of the component of the electric field normal to the piezo surface generated by the normal component of the stress incident on the piezo material), A [m^2] is the sensor surface area, r is a position on the sensor surface, θ_t is the incidence angle of the transmitted acoustic wave inside the piezoelectric material, and T_A is the amplitude transmission coefficient given by:[27]

$$T_A=\frac{\dfrac{2Z_{\text{piezo}}}{\cos\theta_t}}{\dfrac{Z_{\text{piezo}}}{\cos\theta_t}+\dfrac{Z_{\text{tissue}}}{\cos\theta_i}}; \qquad (2)$$

where θ_i is the angle of incidence of the acoustic wave, and Z is the acoustic impedance of the piezo material or tissue.

Numerical evaluation of Eq. (1) yields the voltage response of the sensor to a pressure transient $P(r,t)$. In our calculations the pressure transient generated by a spherical photoacoustic source, as described by Sigrist and Kneubühl[28] and Hoelen and de Mul,[29] was used. This bipolar pressure transient is characterized by its peak-to-peak time τ_{pp} (time difference between the occurrence of the positive and negative peak), the zero-crossing time $\tau=r/v$ (r is the distance from source to detector), and amplitude $P_{\max}$:

$$P(r,t)=-P_{\max}(r)\sqrt{e}\frac{t-\tau}{1/2\tau_{pp}}\exp\left[-\frac{1}{2}\left(\frac{t-\tau}{1/2\tau_{pp}}\right)^2\right]. \qquad (3)$$

Before the signals detected by the two ring-shaped sensor areas can be processed, they have to be corrected for their mutual time delay.

Figure 1 shows the time delays Δt_{in} and Δt_{out}, which appear when a signal travels from a source located on-axis to the inner and outer ring, respectively. By applying this time delay, the time t' at which the signals are detected by the rings is corrected such that the corrected time t corresponds to the depth z of the photoacoustic source ($t=z/v$):

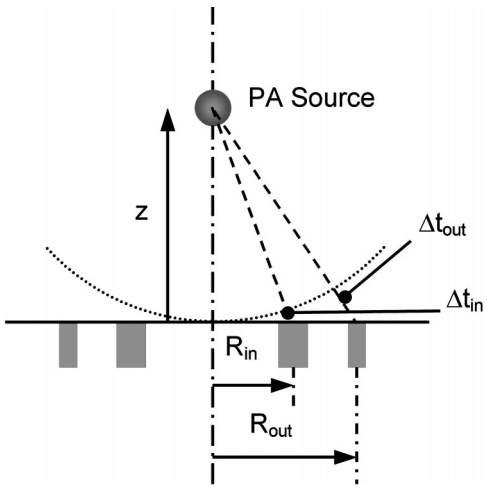

Fig. 1 Schematic overview of time delay for a photoacoustic (PA) signal, traveling from a source located on-axis to the inner and outer rings.

$$t=\frac{[(vt')^2-R_i^2]^{1/2}}{v}, \qquad (4)$$

where R_i is the radius to the center of the inner or outer ring-shaped detection area and v is the velocity of sound. This procedure is comparable to dynamic focusing in ultrasound imaging. Since now the time axes of both rings are corresponding to the depth of the photoacoustic source, the signals of both rings can be processed (e.g., adding the signals).

The directional sensitivity of the sensor was determined theoretically by calculating the maximum amplitude of the sum of the signals detected by the two rings as a function of the distance of the photoacoustic source to the midline of the sensor, while the source was located at a depth of 10 mm.

As depicted in Fig. 2, the double-ring sensor has an angular aperture, which is defined as the arctan of HWHM over depth, of 1.5 deg for photoacoustic signals with a peak-to-peak time of 67 ns, compared to an angular aperture of 2.1 deg for a single (inner) ring. Furthermore, the double-ring sensor shows a detected amplitude generated by sources lo-

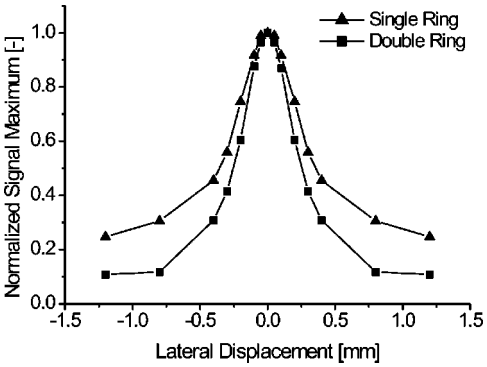

Fig. 2 Theoretically calculated directional sensitivity of the double-ring sensor together with the directional sensitivity of a single ring (inner ring) for a photoacoustic point source located at a depth of 10 mm producing a photoacoustic signal with a peak-to-peak time of 67 ns.

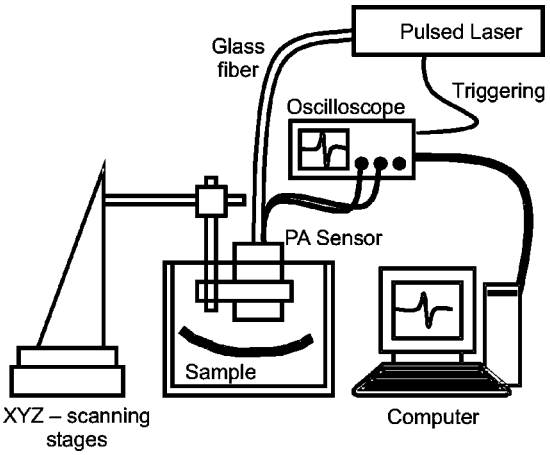

Fig. 3 Setup used to detect photoacoustic signals from absorbing structures (e.g., artificial blood vessels) in a container filled with water or a fluid mimicking optical and acoustic properties of tissue. The container can also be replaced with real tissue (e.g., a human arm) to perform *in vivo* experiments. The photoacoustic (PA) sensor can be scanned in the *xyz* direction with respect to the object.

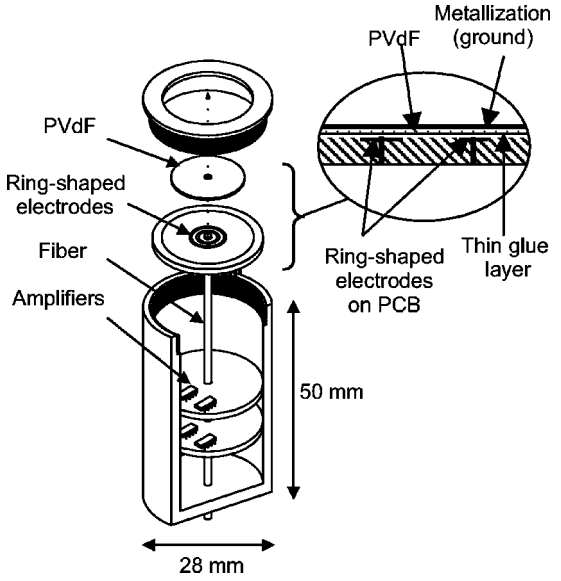

Fig. 4 Schematic drawing of photoacoustic double-ring sensor, with a fiber for illumination integrated in the sensor. The piezo-film (PVdF) is glued to the PCB with two ring-shaped, copper electrodes on it. The top surface of the PVdF is metallized and connected to ground. The pre- and post-amplifiers are mounted inside the brass housing.

cated at a position 1-mm off-axis that is half the amplitude of the photoacoustic (PA) signals detected by a single ring, which means that the double-ring sensor is less sensitive to sources located off-axis.

3 Materials and Methods

3.1 *Setup*

To generate photoacoustic signals, a pulsed light source is required. If this light source generates pulses with a pulse-duration shorter than the acoustic transit time ($=\delta/v$) of the acoustic source (v is the acoustic velocity, δ is the optical absorption depth of laser energy, assuming that the beam diameter is much larger than δ), the condition of stress confinement is fulfilled. When stress confinement is preserved, the maximum possible thermoelastic pressure transient will be generated. A Q-switched Nd:YAG laser (Brilliant B, Quantel, France) was used together with an optical parametric oscillator (OPO, Opotek, USA), which generates light pulses with a duration of about 6 ns, and a repetition rate of 10 Hz. The tuning range of the OPO ranged from 690 to 950 nm. The pulse duration fulfils the requirements of stress confinement when using photoacoustics to localize blood vessels in the visible and near-infrared wavelength range. The light was coupled into a glass fiber, which was integrated in the photoacoustic sensor. A schematic overview of the setup is shown in Fig. 3.

As the sensor has a narrow angular aperture, the measured time traces can be regarded as 1-D depth images [amplitude (A) scans] of photoacoustic sources inside the measurement volume. A 2-D image (scan direction versus depth) is obtained by scanning the sensor over the tissue surface and by plotting all A scans next to each other in a 2-D image plane. This procedure is comparable to an echographic B scan.

The sample (e.g., artificial blood vessel) was placed in a container filled with water or a fluid mimicking optical and acoustic properties of tissue. Instead of using a container with a sample inside, the sensor can also be scanned over a tissue surface (e.g., human arm) to obtain *in vivo* photoacoustic images. Acoustic coupling between the tissue surface and photoacoustic sensor is in this case obtained by using an optical transparent ultrasound contact gel (Sonogel®, Germany). The photoacoustic signals were collected by a dual-channel, digital oscilloscope (TDS220, Tektronix, 1 G sample/s, 100-MHz bandwidth) at a sample rate of 250 Msamples/s, and synchronized (triggered) on the Q-switch trigger generated by the laser.

A schematic drawing of the sensor is shown in Fig. 4. The home-built double-ring sensor consisted of two concentric ring-shaped electrodes with equal area. The piezoelectric material (25-μm-thick PVdF, biaxially stretched, electrically polarized, with one side metallized Au/Pt, Piezotech SA, France) was glued to the electrodes by applying a pressure of about 2.5 MPa during the few seconds directly after gluing to minimize the thickness of the glue layer. The two ring-shaped electrodes were connected to amplifiers. The sensor was embedded in a brass housing to shield the electronics for electromagnetic noise. An optical fiber (core diameter 600 μm, NA=0.22) was placed in the center of the sensor to deliver light pulses to the tissue.

3.2 *Signal Analysis*

3.2.1 *Cross-correlation*

Figure 2 shows that the double-ring sensor detects sources located 1-mm off-axis with amplitude of about 10% compared to the amplitude of sources located on-axis, which is already a factor of 2 less compared to a single ring. The contribution of these off-axis sources can be further suppressed by using the zero-time cross correlation $C(\Delta t=0)=C_0$ [Eq. (5)] between the signals detected by the inner ring $P_{\text{in}}(t)$ and outer ring $P_{\text{out}}(t)$ as a weight factor.

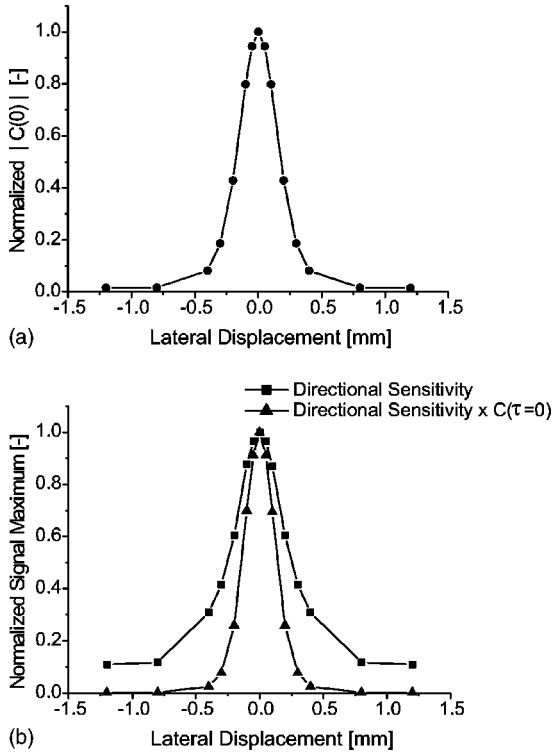

Fig. 5 (a) Theoretically calculated zero- time cross-correlation of the signals detected by the inner and outer ring, as a function of the lateral position of a photoacoustic point source, located at a depth of 10 mm, which generates a signal with a peak-to-peak time of 67 ns. (b) Theoretically calculated directional sensitivity of the double-ring sensor with and without multiplication by the zero-time cross-correlation function as shown in (a).

$$C(\Delta t) = \int P_{\text{in}}(t) P_{\text{out}}(t+\Delta t)\, dt. \tag{5}$$

When the photoacoustic source is located on-axis, and when the photoacoustic signals are corrected for the time delay (i.e., dynamic focusing), the cross correlation C_0 will be maximum, since the corrected signals of both rings will be identical in shape and temporal behavior. When the source is located off-axis, the signals detected by the inner and outer ring will be different in shape and temporal behavior, due to different interference at the inner and outer ring. This difference in temporal behavior and shape, which even can be multipolar instead of bipolar, will cause a decrease of the cross correlation value C_0.

The theoretically calculated zero-time cross correlation C_0 of the signals detected by the inner and outer ring, as a function of lateral position of the photoacoustic source, after correction for the time delay is shown in Fig. 5(a). Using the cross correlation values as a weight factor suppresses the amplitude of signals generated off-axis, as is shown in Fig. 5(b). The plotted theoretical response of the sensor as a function of source translation, with and without multiplication by the zero-time cross correlation values, clearly shows a reduction of the angular aperture by a factor 1.9, from 1.5 to 0.8 deg.

3.2.2 *Absorption imaging*

The output voltage of the photoacoustic sensor is a representation of the photoacoustic pressure transient. In fact, one is not interested in this pressure transient but in the photoacoustic source generating this pressure transient. In this section, the algorithm to reconstruct the absorption distribution of the photoacoustic source from the measured pressure transient will be described.

In the case of a spherical photoacoustic source with a 3-D Gaussian absorption distribution, the initial Gaussian temperature distribution, directly after heating by the laser pulse, is given by

$$\Delta T(x, t=0) = T_{\max} \exp\left[-\frac{1}{2}\left(\frac{x}{1/2v\,\tau_{pp}} \right)^2 \right], \tag{6}$$

with x being the distance from the center of the photoacoustic source, and $r_0 = 1/2\sqrt{2}\,\tau_{pp} v$ being the 1/e radius of the initial Gaussian heat distribution. This initial temperature distribution represents the absorbed energy profile. The resulting pressure transient[28,29] is described by Eq. (3), in which the pressure is given in the form of an amplitude factor $P_{\max}$ times a normalized function. This function is equivalent to the first derivative of a Gaussian function with the retarded time $(t-\tau)$ as variable. Integrating this function [Eq. (3)] over the retarded time [Eq. (6)] will yield a Gaussian function whose shape appears to be equal to the initial Gaussian temperature distribution, i.e., the absorbed energy profile. The time t in the expression for the pressure transient [Eq. (3)] now has to be interpreted in terms of position z (depth), measured from the sensor surface, by multiplying time with the speed of sound ($\sim$1500 m/s) in tissue. Thus, the absorbed energy profile, along the axis of the sensor, is given by

$$\begin{aligned} A(z) &\propto \int_0^{z/v-\tau} P(t-\tau)\, d(t-\tau) \\ &= 1/2 P_{\max} \sqrt{e}\,\tau_{pp} \exp\left[-\frac{1}{2}\left(\frac{z - v\tau}{1/2v\,\tau_{pp}} \right)^2 \right]. \end{aligned} \tag{7}$$

This absorption distribution $A(z)$ is a Gaussian function, which is characterized by its standard deviation or flex point σ (square root of the variance of the distribution), which is equal to $1/2\tau_{pp}$, with τ_{pp} the peak-to-peak time of the detected bipolar pressure transient. Comparison of this equation with the initial Gaussian temperature distribution [Eq. (6)], shows that the Gaussian distributions of these functions have identical dimensions. It has to be noted that in Eq. (7) $(z - v\tau) = (z - r)$, with r being the distance from the source to the sensor surface, and z, a point on the axis of the sensor measured from the sensor surface, is equal to x, which is the distance measured from the center of the photoacoustic source.

In this study, the acoustic signals generated by a blood vessel will be approximated by the previously mentioned model of a spherical photoacoustic source. It is obvious that this is a simple approximation of a blood vessel that is a cylindrical rather than a spherical photoacoustic source. Furthermore, a blood vessel will have a uniform absorption distribution instead of a Gaussian distribution. However, it will be shown that in spite of these shortcomings in our approxi-

mation, satisfactorily reconstructed images of the cross sections of blood vessels are obtained. The only requirement is that the radius of the blood vessel has to be smaller than the absorption mean free path [$=1/\mu_{a,\mathrm{blood}}$, with $\mu_{a,\mathrm{blood}}$ the optical absorption coefficient of blood (mm^{-1})]. For larger radii of the blood vessels, the light-intensity decays too much inside the vessel and only the outer shell of the blood vessel will contribute to the photoacoustic signal. In these cases this model can no longer be used to approximate our photoacoustic signals. If (near) infrared light is used ($\sim$700 to 1100 nm), the absorption of blood will be less than 0.7 mm^{-1}, which results in a maximum vessel radius, for which this approximation will hold, of about 1.5 mm. Fitting the model function [Eq. (3)] to the measured photoacoustic time traces and integrating this fitted function over time (depth) yields the absorption distribution of the vessel. In this way the cross section of a blood vessel is reconstructed.

To suppress the contribution of sources located off-axis and to achieve a narrower angular aperture, the zero-time-shift cross correlation values of the two signals of the separate ring-shaped electrodes were used as weight factors in the image, which implies that each 1-D depth image (A scan) was multiplied by its own weight factor.

In case that multiple structures were present in the same A scan, the fitting procedure was applied to multiple time windows of the A scan.

3.3 *Experiments*

3.3.1 *Sensor characteristics*

The directional sensitivity of the sensor and the cross correlation technique was verified experimentally. A 200-μm-diam, black horse-tail hair, illuminated by a 100-μm-diam fiber ($\lambda = 690$ nm), acted as a photoacoustic point source, generating a bipolar photoacoustic signal with a peak-to-peak time of 40 ns. The hair was illuminated from the bottom side, along a length of about 200 μm. The directional sensitivity was measured by laterally displacing the sensor with respect to the source, while the source was located at a depth of 10 mm. At each measurement position the photoacoustic time traces were averaged 16 times. The maximum amplitude of the photoacoustic signal was taken as a measure for the directional sensitivity.

3.3.2 *Imaging artificial blood vessel*

To demonstrate photoacoustic imaging with the double-ring sensor, an artificial blood vessel in a tissue-like medium was imaged. A silicone rubber tube filled with flowing undiluted human blood (anticoagulated with lithium heparin) acted as an artificial blood vessel. This vessel was immersed in a 7.5% Intralipid-10% dilution, resulting in a reduced scattering coefficient of 0.75 mm^{-1} at a wavelength of 800 nm.[30] The internal diameter of the tube was 1 mm, with a wall thickness of 0.5 mm. The tubing was positioned at a depth of 7 mm with respect to the sensor and was illuminated by the fiber in the center of the photoacoustic sensor. A pulse energy of 1 mJ was applied, with a pulse duration of 8 ns, at a wavelength of 800 nm and a repetition rate of 10 Hz. The signals detected by the sensor were averaged 128 times before being transferred to the computer. A scan perpendicular to the tubing (B scan) was made by 51 subsequent A scans equidistantly positioned with 0.1 mm spacing.

3.3.3 *In vivo imaging*

An *in vivo* experiment on blood vessels in the human wrist was performed by making a B scan consisting of 101 A scans with a spacing of 0.2 mm. To obtain an A scan, at each position 16 photoacoustic time traces were averaged, resulting in a total B-scan time of 5 min. A gap of about 6 mm between the skin and sensor was filled with ultrasound contact gel (Sonogel®, Germany) to ensure good acoustic coupling. Acoustic signals were generated by illuminating the tissue with 1 mJ/pulse at a wavelength of 1064 nm. The energy density at the skin was about 20 $\mathrm{mJ/cm}^2$.

4 Results

4.1 *Sensor Characteristics*

The directional sensitivity of the photoacoustic double-ring sensor was measured and compared with the theoretically calculated curve [Fig. 6(a)]. The zero-time cross correlation values were calculated from the measured data [Fig. 6(b)] and the measured directional sensitivity was multiplied by these cross correlation values [Fig. 6(c)]. By using the zero-time cross correlation as a weight factor, the forward sensitivity of the sensor is more pronounced, i.e., a narrower angular aperture. Furthermore, the contribution of sources located off-axis is suppressed when the cross correlation values are used as weight factors.

4.2 *Imaging Artificial Blood Vessel*

The photoacoustic image of the artificial blood vessel [Fig. 7(a)] was obtained by plotting the absolute values of the photoacoustic time traces (A scans) as 1-D depth images next to each other. The horizontal broadening of the image of the vessel, clearly identified by the lip-like structure in the center of the image, was corrected by using the calculated zero-time cross correlation values from the measured data [Fig. 7(b)] as weight factors to suppress the photoacoustic signals generated off-axis [Fig. 7(c)].

The cross section of the photoacoustic source and thus the artificial blood vessel was reconstructed from the measured photoacoustic time traces. First, the bipolar signal was fitted to the measurement, and next, the fit was multiplied by the zero-time correlation value to reduce lateral broadening of the image [Fig. 8(a)]. Please note that the absolute value of the bipolar fit is plotted, which facilitates positive and negative peaks being depicted in white in the image. By integrating the fitted function over time (depth), the corresponding absorption distribution was calculated [Fig. 8(c)]. Again, the zero-time cross correlation was used as a weight factor. As the size of the vessel was known, the threshold in the image was chosen such that the size of the vessel appearing in the image corresponded to the real size, i.e., this image was used to calibrate our future images. In Fig. 8(c) the upper limit of the grayscale was set to 25% of the maximum value, making everything above this value appear white in the image. To allow comparison of the size of vessels in the images with their actual size, this upper threshold was maintained in all future images. In

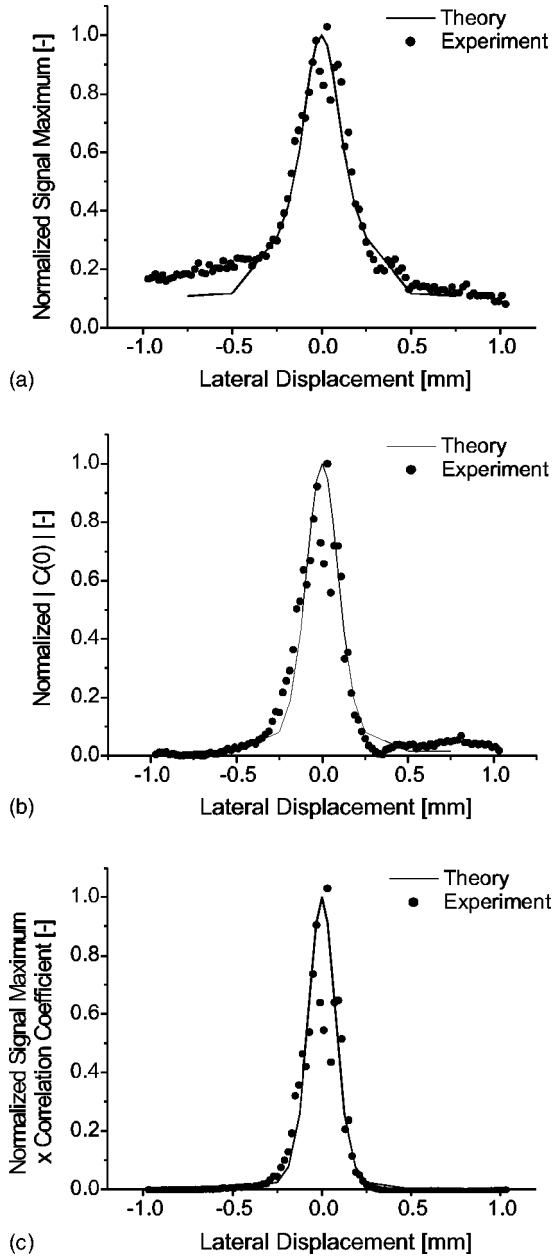

Fig. 6 (a) Measured directional sensitivity defined as the maximum amplitude of the sum of both ring signals, compared with the directional sensitivity calculated from theory, for a point source with a peak-to-peak time of 40 ns, located at 10 mm depth. (b) Cross-correlation values calculated from the measured data as shown in (a), together with the cross-correlation values calculated from theory. (c) Directional sensitivity curve multiplied by the zero-time cross-correlation values resulting from an experiment and resulting from the theoretical calculation.

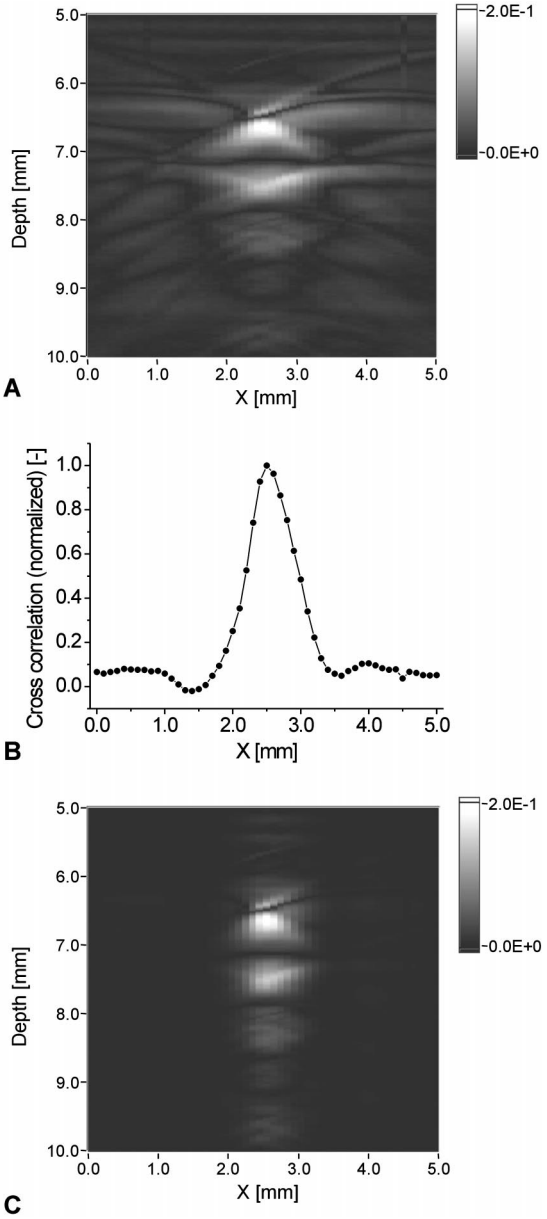

Fig. 7 Photoacoustic image reconstruction of the cross section of a 1-mm-diam silicone rubber tube, filled with human blood, surrounded by 7.5% Intralipid-10% dilution. (a) Photoacoustic image, by plotting the rectified measured time traces (A scans) next to each other. (c) Image after multiplication with the zero-time cross-correlation values shown in graph (b).

Figs. 8(b) and 8(d) cross sections (in depth) of the images in Figs. 8(a) and 8(c) are visualized at positions $X = 2.2$ mm and $X = 2.5$ mm.

4.3 *In Vivo Imaging*

Photoacoustic images of an *in vivo* scan over the human wrist (Fig. 9) revealed, next to the targeted blood vessels, the skin and bone as well. Due to the difference in optical absorption between the ultrasound contact gel (used as an acoustic coupling medium between the skin and the sensor) and the skin, the skin also produced a photoacoustic signal. Below the skin, three superficial blood vessels can be identified in the photoacoustic image. Below these observed vessels, the underlying bone can be recognized. Using the cross-correlation together with the fitting procedure resulted in better visualization of the cross-section of the blood vessels [Fig. 9(b)]. However, while the three blood vessels are clearly present, the skin has almost disappeared.

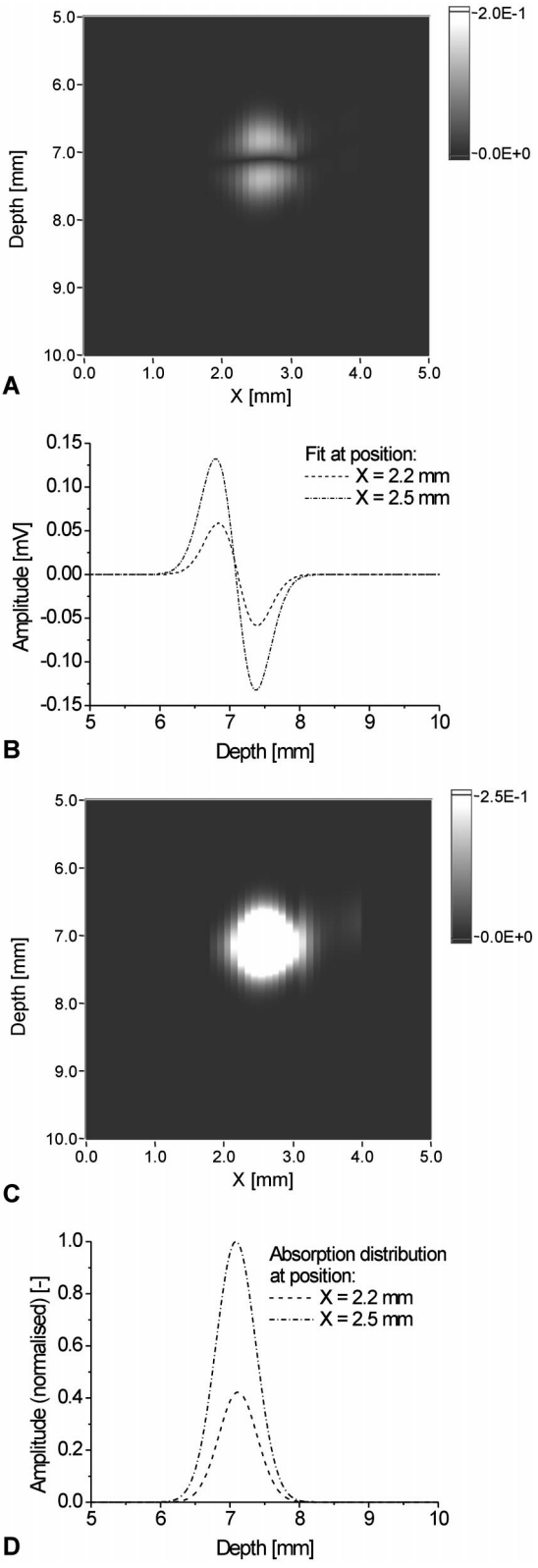

Fig. 8 (a) Photoacoustic image consisting of the bipolar fit to the measurement (Fig. 7), including multiplication with the weight factors based on the zero-time cross-correlation. In the image, the absolute value of the fit is plotted, which facilitates that positive and negative peaks are depicted in white in the image. (c) Image of the absorption distribution after integration of the bipolar fit. Cross-sections (in depth) of images (a) and (c) at positions $X = 2.2$ mm and $X = 2.5$ mm are shown in graphs (b) and (d), respectively.

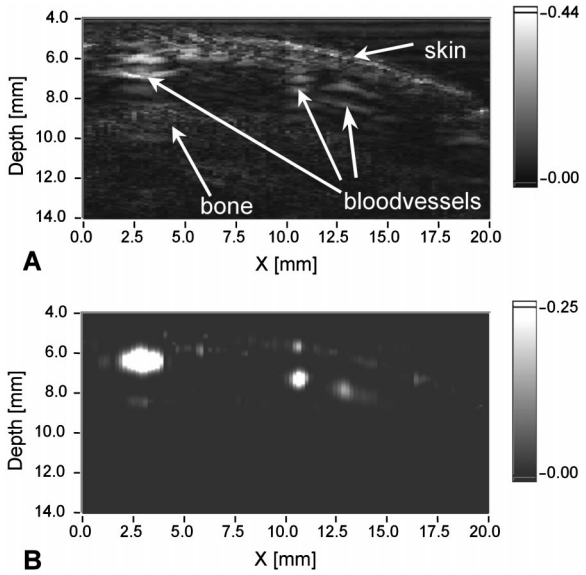

Fig. 9 Photoacoustic image of blood vessels in the wrist of a human volunteer. The image consists of 101 measurement positions along a line (B scan) with a spacing of 0.2 mm. At each measurement position (A scan) the photoacoustic time traces were averaged 16 times. (a) Photoacoustic image before image enhancement; and (b) photoacoustic image after the use of the cross-correlations as weight factors and image enhancement (fitting).

5 Discussion

In this work, the use of a novel double-ring photoacoustic sensor for photoacoustic imaging is demonstrated. This sensor features a narrow angular aperture, which means that the measured time traces can be regarded as individual A scans of the tissue. Performing a B scan with this sensor provides us with 2-D images of optically absorbing structures inside the tissue. Since our sensor operates in reflection mode, it can be applied to various sites of the body to image absorbing structures like blood vessels or tumors. Furthermore, a method to reconstruct the optical-absorption distribution of the photoacoustic sources from single A scans has been applied. As our sensor has a narrow angular aperture, no information of adjacent sensor positions is needed to reconstruct the image, which is in contrast to other photoacoustic image reconstruction algorithms.[21–24]

Both measurements of the directional sensitivity of the double-ring sensor and application of the cross-correlation method showed a good correspondence with theoretical calculations (Fig. 6). However, a decrease in amplitude could be observed for some points in the center (exactly above the hair) of the directional sensitivity curve. As the absorption of the hair was fairly high, only a part, the bottom side, of the hair acted as a photoacoustic source. Furthermore, the hair had acoustic properties different from the surrounding water, so it shielded a part of the sound. Despite these artifacts, our measurements showed that the hair was a good approximation of a photoacoustic point source.

This work illustrated the various steps of our photoacoustic imaging approach. At first, lateral broadening of the image was successfully suppressed by using the cross-correlation values as weight factors. Secondly, the absorption distribution

was reconstructed visualizing the cross section of the vessel. In the final photoacoustic image, the circular shape of the artificial vessel is nicely reconstructed without prior knowledge of the vessel shape. The only assumption was that the photoacoustic time trace generated by a part of a blood vessel could be approximated by a bipolar signal [derivative of a Gaussian function, Eq. (3)]. In our approach, the measurements from different sensor positions of the B scan were treated as independent, individual A scans (1-D depth images), which were plotted as vertical lines [Figs. 8(b) and 8(d)] in the 2-D image. This permitted real-time reconstruction of the image without the need of information of adjacent sensor positions, which are needed in other photoacoustic reconstruction algorithms.[21–24] The lateral resolution is determined by the angular aperture of the sensor, and therefore deteriorates as a function of depth. In the case of a photoacoustic source producing a pressure transient with a peak-to-peak time of 67 ns [Fig. 5(b)], the lateral resolution at a depth of 10 mm will be 280 μm.

The assumption that we can approach the photoacoustic signals of a blood vessel with those from a spherical source requires that the radius of the blood vessel has to be smaller than the absorption mean free path ($=1/\mu_{a,\mathrm{blood}}$). If the case of (near) infrared light ($\sim$700 to 1100 nm) is used, the maximum vessel radius for which this approximation will hold will be about 1.5 mm. For larger vessels, the decaying light intensity inside the vessel has to be taken into account, for instance, as described by the model of Hoelen and de Mul.[29] However, in this case no analytical expression is available that makes the fitting of this model to the measured photoacoustic signals more difficult. The reconstructed absorption distribution can also be used to obtain information about the vessel diameter.

The resulting photoacoustic image of the human wrist demonstrates that superficial blood vessels *in vivo* can be visualized. Besides skin and vessels, the underlying bone is also identified in Fig. 9(a), at a depth of about 3 mm below the skin surface. The depth position of the observed vessels was about 1.5 to 2 mm below the skin surface. The maximum depth at which vessels can be detected is dependent on parameters such as the amount of light applied to the tissue, the wavelength used, and the sensitivity of the photoacoustic sensor.

In a future study, the imaging resolution *in vivo* will be determined by comparison with a reference method such as Doppler ultrasound. However, in preliminary experiments, using the reconstruction algorithm for tubes of various diameters [similar to Fig. 8(c)], we observed that the diameter of the tubes could be estimated with an accuracy of 0.15 mm.

While our correction algorithms are particularly proper for imaging blood vessels, the vanishing of the skin in Fig. 9(b) demonstrates that it is less suitable for visualizing the skin. We hypothesize that these structures, such as skin, generate more complicated signals, which cannot be fitted by Eq. (3). Consequently, such structures are better visible in the uncorrected images.

Currently, the time needed to obtain a 2-D image, consisting of 101 measurement positions (A scans), is about 5 min. At each measurement position, the photoacoustic time traces were averaged 16 times. As the repetition rate of our laser was 10 Hz, this took 1.6 s per measurement position, resulting in a total data acquisition time of 2.7 min. The remaining part of the 5 min was needed for mechanical scanning of the sensor. Increasing the repetition rate to 1 kHz will reduce the averaging time per measurement position with a factor of 100.

6 Conclusions

A novel double-ring photoacoustic sensor is designed and constructed, featuring a narrow angular aperture. Since a fiber for illumination is integrated in the sensor, this sensor could be used in reflection mode. By making a B scan, a 2-D photoacoustic image of absorbing structures hidden in tissue (e.g., blood vessels) is obtained.

It is shown that by using the cross-correlation values between the signals of the inner and the outer ring, the contribution of off-axis sources is suppressed, which reduces lateral broadening of the photoacoustic image. The cross section of blood vessels is reconstructed by fitting a model function to the measured data. Integrating over time (i.e., depth) yields the absorption distribution. This double-ring photoacoustic sensor is successfully applied to *in vivo* imaging of superficial blood vessels in the wrist of a human volunteer.

Acknowledgment

This work was supported by the Netherlands Technology Foundation STW (grant TTN4661) and the Netherlands Foundation of Fundamental Research on Matter FOM (grant 00PMT22).

References

1. C. G. A. Hoelen, F. F. M. de Mul, R. Pongers, and A. Dekker, ''Three-dimensional photoacoustic imaging of blood vessels in tissue,'' *Opt. Lett.* **23**, 648–650 (1998).
2. M. C. Pilatou, N. J. Voogd, F. F. M. de Mul, L. N. A. van Adrichem, and W. Steenbergen, ''Analysis of three-dimensional photoacoustic imaging of a vascular tree in vitro,'' *Rev. Sci. Instrum.* **74**(10), 4495–4499 (2003).
3. R. A. Kruger, W. L. Kiser, D. R. Reinecke, and G. A. Kruger, ''Thermoacoustic computed tomography using a conventional linear transducer array,'' *Med. Phys.* **30**, 856–860 (2003).
4. R. A. Kruger, W. L. Kiser, D. R. Reinecke, G. A. Kruger, and K. D. Miller, ''Thermoacoustic optical molecular imaging of small animals,'' *Molecular Imag.* **2**, 113–123 (2003).
5. X. D. Wang, Y. J. Pang, G. Ku, X. Y. Xie, G. Stoica, and L. V. Wang, ''Noninvasive laser-induced photoacoustic tomography for structural and functional in vivo imaging of the brain,'' *Nat. Biotechnol.* **21**, 803–806 (2003).
6. X. D. Wang, Y. J. Pang, G. Ku, G. Stoica, and L. V. Wang, ''Three-dimensional laser-induced photoacoustic tomography of mouse brain with the skin and skull intact,'' *Opt. Lett.* **28**(19), 1739–1741 (2003).
7. A. A. Oraevsky, A. A. Karabutov, S. V. Solomatin, E. V. Savateeva, V. G. Andreev, Z. Gatalica, H. Singh, and R. D. Fleming, ''Laser optoacoustic imaging of breast cancer in vivo,'' *Proc. SPIE* **4256**, 6–15 (2001).
8. J. A. Viator, G. Au, G. Paltauf, S. L. Jacques, S. A. Prahl, H. Ren, Z. Chen, and J. S. Nelson, ''Clinical testing of a photoacoustic probe for port wine stain depth determination,'' *Lasers Surg. Med.* **30**, 141–148 (2002).
9. G. Paltauf and H. Schmidt-Kloiber, ''Pulsed optoacoustic characterization of layered media,'' *J. Appl. Phys.* **88**(3), 1624–1631 (2000).
10. K. P. Köstli, M. Frenz, H. P. Weber, G. Paltauf, and H. Schmidt-Kloiber, ''Optoacoustic infrared spectroscopy of soft tissue,'' *J. Appl. Phys.* **88**(3), 1632–1637 (2000).
11. R. G. M. Kolkman, E. Hondebrink, W. Steenbergen, and F. F. M. de Mul, ''In vivo photoacoustic imaging of blood vessels using an extreme-narrow aperture sensor,'' *IEEE J. Sel. Top. Quantum Electron.* **9**(2), 343–346 (2003).
12. C. G. A. Hoelen, A. Dekker, and F. F. M. de Mul, ''Detection of

photoacoustic transients originating from microstructures in optically diffuse media such as biological tissue,'' *IEEE Trans. Ultrason. Ferroelectr. Freq. Control* **48**(1), 37–47 (2001).
13. A. A. Karabutov, E. V. Savateeva, N. B. Podymova, and A. A. Oraevsky, ''Backward mode detection of laser-induced wide-band ultrasonic transients with optoacoustic transducer,'' *J. Appl. Phys.* **87**(4), 2003–2014 (2000).
14. V. G. Andreev, A. A. Karabutov, and A. A. Oraevsky, ''Detection of ultrawide-band ultrasound pulses in optoacoustic tomography,'' *IEEE Trans. Ultrason. Ferroelectr. Freq. Control* **50**(10), 1383–1390 (2003).
15. A. A. Oraevsky and A. A. Karabutov, ''Ultimate sensitivity of time resolved opto-acoustic detection,'' *Proc. SPIE* **3916**, 228–239 (2000).
16. G. Paltauf, H. Schmidt-Kloiber, K. P. Köstli, and M. Frenz, ''Optical method for two-dimensional ultrasonic detection,'' *Appl. Phys. Lett.* **75**(8), 1048–1050 (1999).
17. K. P. Köstli, M. Frenz, P. Weber, G. Paltauf, and H. Schmidt-Kloiber, ''Optoacoustic tomography: time-gated measurement of pressure distributions and image reconstruction,'' *Appl. Opt.* **40**(22), 3800–3809 (2001).
18. J. J. Niederhauser, D. Frauchiger, H. P. Weber, and M. Frenz, ''Real-time optoacoustic imaging using a Schlieren transducer,'' *Appl. Phys. Lett.* **81**, 571–573 (2002).
19. P. C. Beard, F. Perennes, and T. N. Mills, ''Transduction mechanisms of the Fabry-Perot polymer film sensing concept, for wideband ultrasound detection,'' *IEEE Trans. Ultrason. Ferroelectr. Freq. Control* **46**(6), 1575–1582 (1999).
20. P. C. Beard, A. M. Hurrel, and T. N. Mills, ''Characterization of a polymer film optical fiber hydrophone for use in the range 1 to 20 MHz: a comparison with PVDF needle and membrane hydrophones,'' *IEEE Trans. Ultrason. Ferroelectr. Freq. Control* **47**(1), 256–264 (2000).
21. C. G. A. Hoelen and F. F. M. de Mul, ''Image reconstruction for photoacoustic scanning of tissue structures,'' *Appl. Opt.* **39**(31), 5872–5883 (2000).
22. M. Xu, Y. Xu, and L. V. Wang, ''Time-domain reconstruction algorithms and numerical simulations for thermoacoustic tomography in various geometries,'' *IEEE Trans. Biomed. Eng.* **50**(9), 1086–1099 (2003).
23. K. P. Köstli, D. Frauchiger, J. J. Niederhauser, G. Paltauf, H. P. Weber, and M. Frenz, ''Optoacoustic imaging using a three-dimensional reconstruction algorithm,'' *IEEE J. Sel. Top. Quantum Electron.* **7**(6), 918–923 (2001).
24. K. P. Köstli and P. C. Beard, ''Two dimensional photoacoustic imaging by use of Fourier-transform image reconstruction and a detector with an anisotropic response,'' *Appl. Opt.* **42**(10), 1899–1908 (2003).
25. R. G. M. Kolkman, M. C. Pilatou, E. Hondebrink, and F. F. M. de Mul, ''Photo-acoustic A-scanning and monitoring of blood content in tissue,'' *Proc. SPIE* **3916**, 76–83 (2000).
26. K. P. Köstli, M. Frenz, H. P. Weber, G. Paltauf, and H. Schmidt-Kloiber, ''Pulsed optoacoustic tomography of soft tissue with a piezoelectric ring sensor,'' *Proc. SPIE* **3916**, 67–74 (2000).
27. V. M. Ristic, *Principles of Acoustic Devices*, J. Wiley and Sons, New York (1983).
28. M. W. Sigrist and F. K. Kneubühl, ''Laser generated stress waves in liquids,'' *J. Acoust. Soc. Am.* **64**, 1652–1663 (1978).
29. C. G. A. Hoelen and F. F. M. de Mul, ''A new theoretical approach to photoacoustic signal generation,'' *J. Acoust. Soc. Am.* **106**(2), 695–706 (1999).
30. H. J. van Staveren, C. J. M. Moes, J. van Marle, S. A. Prahl, and M. J. C. van Gemert, ''Light scattering in Intralipid-10% in the wavelength range of 400–1100 nm,'' *Appl. Opt.* **30**, 4507–4514 (1991).